Bulletin of Earthquake Engineering

Centrifuge modelling of the seismic performance of soft buried barriers

--Manuscript Draft--

Manuscript Number:	
Full Title:	Centrifuge modelling of the seismic performance of soft buried barriers
Article Type:	Original Research
Keywords:	seismic risk, risk mitigation, soft grouted barrier, centrifuge tests, numerical analyses
Corresponding Author:	Valeria Nappa, Ph.D. student Universita degli Studi di Napoli Federico II Napoli, ITALY
Corresponding Author Secondary Information:	
Corresponding Author's Institution:	Universita degli Studi di Napoli Federico II
Corresponding Author's Secondary Institution:	
First Author:	Valeria Nappa, Ph.D. student
First Author Secondary Information:	
Order of Authors:	Valeria Nappa, Ph.D. student
	Emilio Bilotta, Assistant Professor, Ph.D
	Alessandro Flora, Associate Professor, Ph. D
	Gopal Madabhushi, Reader, Ph.D.
Order of Authors Secondary Information:	
Funding Information:	
Abstract:	The paper presents the results of an experimental work carried out in a geotechnical centrifuge at the Schofield Centre of Cambridge University. Two reduced scale models of soft barriers in a sand layer underwent a series of ground shaking. In the first model a thin horizontal layer made of latex balloons filled with a cross-linked gel was created at about mid-height of the sand layer. In the second, the same balloons were deployed to form a V-shaped barrier aimed at isolating a relatively shallow volume of sand. The aim of the study was to get experimental evidence of the capability of such soft barriers to isolate a volume of soil thus reducing ground amplification during ground motion caused by earthquakes. The experimental results were compared with FE numerical analyses of the same models, carried out also in free field to have a benchmark condition. By validating the FE modelling via the comparison with the experimental results, a robust model has been built, aimed at being used for carrying out a wider parametric numerical testing. The experimental results confirm the effectiveness of such soft barriers to reduce amplification in the isolated volumes during seismic events.
Suggested Reviewers:	Kyriazis Pitilakis pitilakis@civil.auth.gr
	Sebastiano Rampello sebastiano.rampello@uniroma1.it

Centrifuge modelling of the seismic performance of soft buried barriers

Valeria Nappa[1], Emilio Bilotta[2], Alessandro Flora[3], S.P. Gopal Madabhushi[4]

[1]Department of Civil, Architectural and Environmental Engineering, University of Napoli Federico II, via Claudio 21, 80125 Naples (Italy)
e-mail: valeria.nappa@unina.it
Tel. (+39) 081 768 3617 -fax (+39) 081 768 3481

[2]Department of Civil, Architectural and Environmental Engineering, University of Napoli Federico II, via Claudio 21, 80125 Naples (Italy)
e-mail: emilio.bilotta@unina.it

[3]Department of Civil, Architectural and Environmental Engineering, University of Napoli Federico II, via Claudio 21, 80125 Naples (Italy)
e-mail: alessandro.flora@unina.it

[4]Schofield Centre, University of Cambridge, High Cross, Madingley Road, Cambridge (UK)
e-mail: mspg1@cam.ac.uk

Abstract

The paper presents the results of an experimental work carried out in a geotechnical centrifuge at the Schofield Centre of Cambridge University. Two reduced scale models of soft barriers in a sand layer underwent a series of ground shaking. In the first model a thin horizontal layer made of latex balloons filled with a cross-linked gel was created at about mid-height of the sand layer. In the second, the same balloons were deployed to form a V-shaped barrier aimed at isolating a relatively shallow volume of sand. The aim of the study was to get experimental evidence of the capability of such soft barriers to isolate a volume of soil thus reducing ground amplification during ground motion caused by earthquakes. The experimental results were compared with FE numerical analyses of the same models, carried out also in free field to have a benchmark condition. By validating the FE modelling via the comparison with the experimental results, a robust model has been built, aimed at being used for carrying out a wider parametric numerical testing. The experimental results confirm the effectiveness of such soft barriers to reduce amplification in the isolated volumes during seismic events.

Keywords: seismic risk, risk mitigation, soft grouted barrier, centrifuge tests, numerical analyses

Acknowledgements
The research activity was carried out at the University of Napoli Federico II as part of the national research project PON_03 METRICS. The financial support of the consortium Stress s.c.a r.l. is kindly acknowledged.

1. Introduction

Technological interventions into the ground to mitigate the effects of vibrations have been employed in the past, mostly with reference to the effects of anthropic actions (e.g. surface vibrations induced by vehicles and rail-bound traffic). To this aim, completely different solutions have been studied, all with the aim to modify the impedance ratio α, defined as the dimensionless ratio between the dynamic impedance of the natural and of the treated soil ($\alpha=\eta_s/\eta_g$): for instance creating a stiff layer (high impedance, low value of α under the building to protect, as suggested by Chouw and Schmid, 1992; Kellezi, 2011) or installing vertical wave absorbing barriers close to the vibration source (low impedance, high value of α, using in-filled walls or gas cushion trenches as proposed by Massarsch, 2003 and Massarsch, 2005).
For buildings, the concept of vibration screening was initially proposed by Woods (1968). Interception, scattering, and diffraction of surface waves can be achieved by using barriers such as trenches, sheet-pile walls, and piles (Liao & Sangrey, 1978).
With specific reference to the protection of structures from seismic shaking, different technological means have been considered in literature: for instance, smooth synthetic liners have been proposed underneath the foundation of structures or between soil layers for dissipating seismic energy through sliding (Yegian and

Kadakal, 2004). A potential seismic isolation method, that makes use of scrap rubber tires for the protection of low-to-medium-rise buildings was proposed among others by Tsang (2011). The method involves mixing shredded rubber tire particles with soil materials and placing the mixtures around building foundations, which provides a function similar to that of a cushion.

More recently, the use of soft and weak buried barriers has been proposed (e.g. Kirtas et al., 2009a, 2009b). By introducing flexible deformable vertical diaphragm walls together with a soft horizontal layer in the foundation subsoil, the input ground motion characteristics would be altered, and the structural demand reduced. The adoption of a soft and weak buried barrier bounding a soil volume underneath the foundations of a building is extremely interesting, as theoretically feasible underneath existing structures. This paper will discuss such a kind of solution to reduce seismic shaking at ground level.

Kirtas et al. (2009a, 2009b) first and then Lombardi (2014) have shown that in order to have an effective modification of shear waves propagation, the mass of soil to be protected has to be completely bounded by the soft and weak layer, i.e. the barrier must be continuous to ground level. Based on this finding, numerical parametric analyses have been carried out in order to study the feasibility of the soft barrier and its geometrical and mechanical properties, which optimize the results both in static and in dynamic field (Lombardi et al., 2014; Flora & Lombardi, submitted to Acta Geotechnica for possible publication). The results have shown that there is a range of values of the parameters in which the barrier can be effective as seismic isolation without inducing excessive static settlements. A suitable material to create such a low impedance barrier is for instance a hydrophilic polymer (Super Absorbent Polymer SAP) that can absorb and retain extremely large amounts of a liquid with respect to its own mass (Flora et al., 2015). Its configuration after hydration is that of a cross-linked gel with a density close to that of water. On this material, geotechnical lab tests were carried out in order to obtain the properties necessary to the implementation of numerical analyses. Due to the very low consistency of such a material, specimen preparation was very difficult, hence some uncertainties arose on the measured properties. The results of plane strain dynamic analyses reported in literature (Flora & Lombardi, submitted to Acta Geotechnica for possible publication) also showed that such a soft grouted layer tends to filter the high frequency components of the input signal without modifying in a significant way the low frequency components.

Given the possible uncertainty on the polymer properties measured in the lab, centrifuge experiments on physical models of similar barriers at reduced scale were used to further support the numerical evidence of their effectiveness. The tests were carried out at the Schofield Centre of Cambridge University on two models. In the first model, the soft layer was horizontal, while in the second one a V-shaped barrier was created in the ground.

In the first part of the paper the centrifuge models are described and an interpretation of pulse tests carried out during the centrifuge tests is shown, aimed at obtaining the shear wave velocity profile in the models. This was necessary to the interpretation of the centrifuge testing results and for the subsequent numerical analyses.

Then the main results of tests are shown in terms of ground displacement and acceleration and compared with the numerical results of modelling free-field conditions (without barriers).

Finally, the effectiveness of the two barriers to reduce the ground surface amplification is shown and discussed.

2. Centrifuge tests

2.1. Test Setup and Model Preparation

The tests were carried out in the 10-m diameter Turner beam centrifuge (Madabhushi, 2014). The experimental programme included two tests on a model with different configuration of the soft barrier, performed at two levels of centrifugal acceleration in a special container known as laminar box. The concept of the laminar model container is that it has zero lateral stiffness of its own and therefore its deformation is driven by soil deformation (Scott, 1994; Brennan et al., 2006). The box is made by individual laminas that are separated by cylindrical bearings, so as to minimize the friction. The model container has nominal inside dimensions of $500mm \times 250mm \times 300mm$. A dynamic actuator (Stored Angular Momentum, SAM) was used to fire the model earthquakes (Madabhushi et al., 1998). The SAM actuator works by spinning two flywheels up to the required speed. A clutch mechanism then grabs hold of a reciprocating rod coming from the flywheels which transmits shaking into the model until the clutch releases. The duration, frequency and magnitude of the earthquake can be set independently while the centrifuge is spinning. During a test, each model was subjected to eight earthquakes, consisting of approximately sinusoidal waves with constant duration and different nominal frequency and amplitude. The basic scaling law for centrifuge modelling

derives from the need to ensure the stress similarity between a model and the corresponding prototype. Therefore all the length dimensions of the prototype are scaled down by a factor N in the centrifuge model. The gravity is increased by the same geometric factor N relative to the normal Earth's gravity field. A number of scaling laws is needed to convert between prototype and model (Madabhushi, 2014). Those used for the tests are summarized in Table 1. It is worth noting that both the amplitude and the frequency of the ground motion applied at the base of the model must be N times larger than at the prototype scale.

Table 1
Scaling laws

Parameter	Scaling law Model/Prototype	Dimensions
Length	1/N	L
Mass	1/N3	M
Stress	1	$ML^{-1}T^{-2}$
Strain	1	1
Time (Dynamic)	1/N	T
Frequency	N	T^{-1}
Acceleration	N	LT^{-2}
Velocity	1	LT^{-1}
Displacement	1/N	L

The soil models were made of uniform dry sand, namely HN31 Hostun sand. Table 2 reports its properties as know from existing literature (Flavigny, 1990).

Table 2
Properties of Hostun sand.

Soil	G_s	e_{max}	e_{min}	d_{50} (mm)	d_{10} (mm)	d_{60}/d_{10}
HN31 Hostun Sand	2.65	1.041	0.555	0.335	0.209	1.74

The sand layers were deposited at nominal relative density (D_r) equal to 85%. An automatic sand pourer was used for pluviating the sand in the laminar box. To achieve a specific relative density the sand needs to be poured from a particular height and at a particular flow rate. The sand is placed in a hopper suspended above the model container. A nozzle was placed at the bottom of the hopper to control the flow rate and the drop height was controlled through the program used to control the equipment (Madabhushi et al., 2006)
The soft barrier was made in both of models by latex balloons filled up with the SAP. The reason of confining the SAP inside the balloons is of avoiding that the material would be squeezed during the spin up thus mixing up with the sand in an uncontrolled way. Table 3 reports the properties of the material evaluated by geotechnical lab tests (Flora et al., 2015).

Table 3

Main properties of the SAP material.

Material	γ (kN/m^3)	ρ (kg/m^3)	V_s(m/s)
SAP	10	1020	20

The sand pourer was stopped at desired locations to allow placement of instruments and balloons. In the first model the balloons were deployed between two thin layers of latex. A small hollow tube was placed on the superior layer of latex in order to allow placement of a LVDT as a means of control for the deformation of

the soft layer during the spin up. For the creation of the V-shape model (second model) the sand pouring was stopped every 10 mm in order to place the balloons. For this reason it was impossible to place the two thin layers of latex around the balloons in the second model. The instrumentation adopted in both models is the same. Two sets of accelerometers were installed to measure horizontal and vertical components of acceleration. Piezoelectric accelerometers are the traditional kind of transducers used to measure acceleration in dynamic centrifuge experiments. When they are subjected to vibration, a crystal within the instrument is squeezed which in turns releases a charge. This charge output is converted into a voltage using a charge amplifier. These devices are calibrated before use in a centrifuge test using a specially designed calibrator. Furthermore, Micro-electro-mechanical System (MEMS) accelerometers were installed. These devices have a tiny inertial mass suspended on a spring and their displacements is used to determine the spring force and hence the acceleration of the device. Displacements measurement was carried out traditionally by using linearly varying differential transformer (LVDTs). These devices have a relatively slow response time meaning they are ineffective at measuring high frequency displacements accurately. They do however provide an accurate indication of the cumulative settlement. Prior to use, the LVDTs were calibrated by applying know displacements from a screw gauge and its output was measured. In the end, an air hammer was placed at the bottom of the models to create a shear wave travelling between two accelerometers placed at a known distance apart. Because the shear strain developed during the air hammer test was small, the values of the shear modulus were interpreted as values of initial shear modulus, G_0 (Ghosh and Madabhushi, 2002). The tests were performed after accelerating the models to 50g and 80g. According to the centrifuge scale factors, the two levels of acceleration correspond to the behaviour of two different prototypes (Fig.1).

2.2. Testing programme

As above mentioned, 8 earthquakes were fired for each model, at two different levels of gravity acceleration, g. Table 4 shows the value of amplitude, nominal frequency and duration of each signal both at model and prototype scale. It is worth noting that the SAM cannot achieve higher nominal frequencies.

Table 4
Model earthquakes; a) Horizontal barrier, b) V-barrier.

Model 1							
Input signal	Gravity level (g)	Frequency (Hz)		Duration (s)		Amplitude (g)	
EQ1	50	50	(1)	0.4	(20)	4.6	(0.09)
EQ2	50	30	(0.6)	0.4	(20)	0.6	(0.01)
EQ3	80	50	(0.625)	0.4	(32)	2.6	(0.03)
EQ4	80	50	(0.625)	0.4	(32)	9.8	(0.12)
EQ5	80	30	(0.375)	0.4	(32)	1.9	(0.023)
EQ6	80	60	(0.75)	0.4	(32)	0.7	(0.008)
EQ7	80	60	(0.75)	0.4	(32)	16.5	(0.21)
EQ8	80	30	(0.375)	0.4	(32)	4.5	(0.05)

a)

Model 2							
Input signal	Gravity level (g)	Frequency (Hz)		Duration (s)		Amplitude (g)	
EQ1	80	50	(0.625)	0.4	(20)	7.4	(0.09)
EQ2	80	50	(0.625)	0.4	(20)	13.4	(0.16)
EQ3	80	30	(0.375)	0.4	(32)	1.3	(0.02)
EQ4	80	60	(0.75)	0.4	(32)	13.2	(0.16)
EQ5	80	60	(0.75)	0.4	(32)	19.1	(0.24)
EQ6	80	30	(0.375)	0.4	(32)	4.5	(0.06)
EQ7	50	50	(1)	0.4	(32)	4.1	(0.08)
EQ8	50	30	(0.6)	0.4	(32)	4.5	(0.09)

b)

3. Evaluation of soil properties

Shear wave velocity in the ground, V_S, can be used to evaluate in-flight dynamic soil properties in centrifuge models as in situ. The maximum shear modulus, G_{max}, can be computed from the shear wave velocity in accordance with elastic theory:

$$G_{max} = \rho \cdot V_S^2 \quad (1)$$

where ρ is the mass density of the soil.

In centrifuge tests, the shear wave velocity, V_S, can be measured by using a miniature air hammer, which operates at strain levels around 0.03%. Hence V_S, can be obtained by measuring the time, T, required for the wave to travel between two consecutive accelerometers, and the distance, L, between this two. That is:

$$V_S = \frac{L}{T} \quad (2)$$

In order to evaluate the shear wave velocity in the sand, the second model has been used, where a free-field vertical array of horizontal accelerometers was available.

The distance between the accelerometers A4 and A6 is L=0.07 m and the time lag is T=0.0002 s (L=5.6 m and the time lag is T=0.016 s, at prototype scale), yielding a value of V_S=350 m/s, representative of the shear wave velocity at mid-height of the sand layer, hence from Eq (1) G_{max}= 202 MPa (Fig. 2).

Two air hammer tests were performed in total, at two different g levels (50g and 80g). The shear wave velocities measured at a certain depth and at a specific g level, correspond to the shear wave velocity measured at the corresponding prototype depth. Therefore the prototype V_S profile along the depth could be determined.

From the correlation of Hardin & Black (1969) modified for the Hostun sand (Hoque and Tatsuoka, 2000) as:

$$G_{max} = 80 \cdot \frac{(2.17-e)^2}{(1+e)} \cdot \left(\frac{p'}{p_{ref}}\right)^{0.47} \quad (3)$$

the profile of G with the depth was obtained, hence the shear wave velocity profile (Fig 3). It can be noted that the experimental data are in good agreement with the literature data.

By taking advantage of the air hammer, it is also possible to assess the shear wave velocity in the SAP, by applying a similar procedure to the signals recorded by the accelerometers A4 (below) and A3 (above) the soft barrier, shown in Figure 4.

Since this travel time, t, depends not only on the soft barrier ($t_2 = V_{S,2} \cdot L_2$ in Figure 4) but also on the sand between the two accelerometers ($t_1 = V_{S,1} \cdot L_1$ and $t_3 = V_{S,3} \cdot L_3$ in Figure 5), it is possible to estimate an average shear wave velocity of the barrier as:

$$V_{s,2} = \frac{L_2}{t - \frac{L_1}{V_{s,1}} - \frac{L_3}{V_{s,3}}} \quad (4)$$

where $t = t_1+t_2+t_3$, and the values of the shear wave velocity of the sand, $V_{S,1}$ and $V_{S,3}$ were estimated both from Fig. 3. In order to calculate Vs,2, the thickness of the soft stratum L_2 has to be known, as shown in §5.1.

The soil equivalent shear modulus and damping ratio were evaluated from stress strain cycles. The shear stress and the shear strain histories were evaluated using the procedure proposed by Zeghal & Elgamal (1994). Brennan et al. (2005) described the procedure to calculate shear modulus and damping ratio from stress strain loops in centrifuge tests, derived from the method proposed by Zeghal & Elgamal (1994). The shear stress at any depth was estimated by integrating the equation of an idealized 1D shear beam as:

$$\tau(z) = \int_0^z \rho a dz \quad (5)$$

where z in the depth coordinate, a is the horizontal acceleration and ρ in the density of the material. Linear interpolation of the acceleration was employed to evaluate the shear stress at each level.
The shear strain can be obtained from the relative displacement between two consecutive accelerometers divided by their distance, using a first- or second-order approximation, depending on the number of accelerometers used in the centrifuge test.
Shear modulus and damping ratio mobilized during each earthquake can be evaluated from stress strain loop as:

$$G(\gamma_{max}) = \frac{\tau(\gamma_{max})}{\gamma_{max}}, D = \frac{W_D(\gamma_{max})}{4\,\pi\,W_E} \quad (6)$$

where γ_{max} is the maximum shear strain computed during the earthquake, τ (γ_{max}) the associated shear stress, W_D the energy dissipated during one representative stress-strain cycle, and W_E is the strain energy. As an alternative, Brennan et al. (2005) suggested computing G as the ratio between the difference in maximum and minimum stress applied during a loop and the difference in maximum and minimum strain developed in that loop. Fig 15 shows the stress strain cycle computed during the earthquakes fired at 80 g level on the first model with the calculated shear modulus and damping.
In the second model (Fig 16) it was possible to evaluate the stress strain cycles only along the array 2, due to the malfunctioning of some of the horizontal accelerometers of array 1.
Shear modulus values were derived from three accelerometers aligned vertically below the soft layer in both models (A10, A11, A12). The shear modulus degradation curve are shown in Figure 7 and are compared with the curve generated from the empirical relationship given by Santos and Correia (2011):

$$\frac{G}{G_0} = \frac{1}{1+a\frac{\gamma}{\gamma_{0.7}}} \quad (7)$$

where a is equal to 0.385 and $\gamma_{0.7}$ is the shear strain level at which the secant shear modulus is reduced to about 70% of G_0.

The local hysteretic damping has been calculated with the formulation suggested by Brinkgreve et al. (2007), developed for HS small model in Plaxis. As soon as G_{ur} is reached the damping does not further increase, where G_{ur} is defined as:

$$G_{ur} = \frac{E_{ur}}{2(1+\nu_{ur})} \quad (8)$$

4. Complementing numerical analysis

Numerical simulations of the two centrifuge models were performed by the FE code Plaxis 2D (Brinkgreve, 2013). The geometry of both centrifuge models was reproduced. Additionally the same sand layer without the soft barrier was modelled, in order to have a reference free-field model for comparison.

The soil was characterized by a constitutive model implemented in the Plaxis code, Hardening Soil with small strain overlay, that accounts for strain hardening plasticity and small-strain behaviour of soils (Schanz et al., 1999; Benz et al., 2009). The model is also able to capture the hysteretic behaviour of sand and the associated hysteretic damping in unloading-reloading cycles. Both stiffness decay and hysteretic damping are crucial in the prediction of the stress-strain behaviour of soil under cycling, as in the case of shaking due to earthquakes. Two are needed to describe stiffness from very small to medium strains the initial modulus G_0 and the shear strain level $\gamma_{0.7}$ at which the secant shear modulus is reduced to about 70% of G_0. The model parameters for HN31 Hostun sand were extracted from literature (Benz, 2007) and they are reported in Table 5. The reference pressure p_{ref} is 100 kPa. The value of the parameter E_0^{ref} is consistent with the results shown in Figure 3. The small-strain damping of the sand (D_0) was assumed equal to 0.5%. It was modelled through the Rayleigh formulation, through the coefficient α_R and β_R, estimated using the "double frequency approach" suggested by Park and Hashash (2004). It is worth noting that several procedures can be followed when implementing such an approach. For instance, Amorosi et al. (2010) suggested an iterative procedure, taking into account also the amplification function between the surface and the base level. This seemed

necessary to avoid significant under-damping in the frequency range characterized by an amplification factor larger than one. However, since the Rayleigh formulation was here adopted to model the small-strain damping only (not the hysteretic one at larger strain level), this appeared to be a minor issue. Hence, the parameters were simply calculated by assuming the Rayleigh damping coincident with the initial damping ratio, D_0, at the predominant frequency of the input signal (cf. Table 4) and at the first natural frequency of the soil layer (Lanzano et al., 2015).

Table 5
Hardening Soil Small Strain parameters adopted for the sand

E_{50}^{ref}	E_{oed}^{ref}	E_{ur}^{ref}	m	c	φ	ψ	ν	p^{ref}	K_0^{nc}	E_0^{ref}	$\gamma_{0.7}$
(kN/m^2)	(kN/m^2)	(kN/m^2)	(-)	(kN/m^2)	(°)	(°)	(-)	(kN/m^2)	(-)	(kN/m^2)	(-)
30000	30000	90000	0.55	0	42	16	0.25	100	0.4	270000	0.0002

The soft barrier was modelled as an elastic-perfectly plastic Mohr-Coulomb material. Its shear strength was determined through shear tests (Flora et al., 2015) while the elastic shear wave velocity was obtained by means of air-hammer pulse tests during the centrifuge flight, as shown in the previous section. The adopted values of parameters are summarized in Tab. 6. The small-strain damping of the barrier (D_0) was derived from back-analysis and was assumed equal to 2.5%.

Table 6
Mohr-Coulomb parameters adopted for the soft barrier

ρ	G	φ	ν	V_s
(kN/m^3)	(kN/m^2)	(°)	(-)	(m/s)
1020	109	10	0.4	12

The recorded time history at the base of the centrifuge container was used as the base input motion at the bottom boundary of the FE mesh, schematically shown in Fig 8. Boundary conditions reproduced those of the laminar box used in the tests: periodic boundary at the lateral sides, through displacement restraints between the corresponding nodes, and reflective boundary at the base, through simple supports.

5. Experimental results

5.1. Settlements

The LVDT devices measured the settlements w at two different points in each model, during the centrifuge spin up and the following shakings. The position of the devices was different in the two models, as shown in the insets of Figures 6 and 7. In the first model, an LVDT was placed on the soft barrier to evaluate the settlement of the soft layer due to the increasing self-weight during swing up when the centrifuge was subsequently accelerated in steps of 10g until it reached a gravity of 80g.
As shown in Figure 9, during the swing up, the LVDT 1 (located on the soft layer) showed slightly larger settlement than the LVDT 2. The measurements are referred to two different positions of the LVDTs in the model, one directly placed on the soft layer and the other at ground level. The two measurements are similar. Since it is reasonable to assume that the deformation of the soft layer is much higher than the one of the sand on top, the average value of the two measured settlements reported in Fig. 6 allow to quantify the change of thickness of the soft layer. Under 50 g, before the earthquakes were fired, its thickness is about 12 mm, corresponding to 0.6 m at prototype scale. Such a value was used in Eq. (4) to calculate the shear wave velocity of the soft layer. In particular, by assigning to the sand the relevant shear wave velocities $V_{s,1}$ and $V_{s,3}$ (Fig. 3), the values $V_{s,2}$=11.8 m/s (considering for the sand the shear wave velocity distribution curve proposed by Hoque & Tatsuoka, 2000) and 12.2 m/s (experimentally measured shear wave velocity of the sand) were calculated. The two values are rather close, and therefore the average value of shear wave velocity equal to 12 m/s has been assumed for the soft layer in the following numerical analyses.

At this gravity level, two earthquakes were fired, with different nominal frequencies (cf. Table 3). Finally, the centrifuge was swung up to 80g. According to the LVDT readings, the barrier thickness became equal to 0.9 m at prototype scale. At this new gravity level the remaining earthquakes were fired (cf. Table 3).
In the second model, the LVDT 1 was located at the middle of the model ground surface and LVDT 2 along the free field vertical (Fig. 10). The recorded settlement was larger within the isolated volume (LVDT 1), especially after that all the five earthquakes had been fired.

5.2. Horizontal accelerations

5.2.1. First Model – horizontal barrier

Two vertical arrays of six accelerometers each were installed in the first model (horizontal barrier), three above and three below the soft layer. The first array was aligned to the centreline of the model, the second one was located 75 mm away from one side of the box. One of the external accelerometers, located at the base plate (A14 in Fig. 1), measured the input motion. In Fig. 11 some of the acceleration time histories recorded by A14, and characterized by different nominal frequencies, are shown together with the corresponding Fourier spectra, at prototype scale.
It is evident from the Fourier spectra that the input signals were not exactly harmonic. It may also be noticed that the duration of the shaking events characterized by small amplitude is generally longer than the nominal value of 0.4 s, due to a known issue of the SAM actuator already observed in previous experimental campaigns (e.g. Lanzano et al., 2012). Figs. 12a and b show the acceleration amplification (peak recorded accelerations normalized by the corresponding base peak acceleration) at different depths for all earthquakes, obtained from 50g and 80g models respectively. It can be noted that the acceleration under the soft layer was generally more amplified during weaker excitations. Soon above the barrier attenuation is always observed, although during weaker events it may be not large enough to overcome the amplification induced in the sand layer below the barrier. On the other hand, in case of stronger events, attenuation always occurred, the higher the nominal frequency of the input signal.
The reference free-field conditions to be compared to the test results were established by means of the complementing FE analyses shortly introduced in section 4.
In order to check the reliability of the numerical model, the centrifuge test on the model with horizontal barrier was first simulated. The numerical mesh shown in Fig. 8(b) was adopted in this case. Figure 13 shows, as an example, the results of such calculations for the earthquake 7, since it showed the largest effectiveness of the barrier, thus implicating that an important influence of constitutive non-linearity should be expected in the numerical model. In the same figure the experimental results are shown for comparison. It can be observed that calculated and recorded acceleration time histories at two different depths and the corresponding Fourier spectra are in good agreement between each other, indicating the soundness of the numerical model. Hence the numerical calculations were performed in free field conditions by removing the horizontal barrier from the model, i.e. using the mesh in Figure 8(a).
Fig 14 shows a comparison between the reference (calculated) free-field behaviour and the behaviour during the centrifuge test on the model with horizontal barrier. The results are compared in terms of amplification ratio between the maximum acceleration at surface with ($a_{max,hb}$) and without ($a_{max,ff}$) horizontal barrier, plotted as a function of the peak input acceleration (Fig. 14a) and of the input nominal frequency (Fig. 14b). The results confirm that the barrier is generally more effective during strong earthquakes (amplification ratio lower than 1, in some cases even lower than 0.5). In this case the experimental amplification ratio with the barrier is 2.5 while the numerical free-field calculation yields 2.2.

5.2.2. Second Model V-barrier

As in the model with the horizontal barrier, also in the model with V-shaped barrier two arrays of six accelerometers each were deployed, one (array 1) along the vertical centreline of the model (A1 to A6 in Fig. 1) and the other (array 2) on a side outside the isolated volume of sand (A7 to A12 in Fig. 1). Hence, in this model an immediate comparison is possible between the results along a vertical line that crosses the soft barrier and another that does not. However, the latter array (array 2) is not really in free-field conditions, since it may be influenced by the presence of the barrier aside. For this reason, numerical simulation of the V-shaped barrier model were also carried out, using the numerical mesh of Fig. 8(c). The results achieved for array 2 were hence compared with the results of the reference free-field numerical model (Fig. 8(a)).

Figure 15 shows the acceleration amplification ratio at different depths, for all earthquakes at 80g level only, along both arrays. During the test some of piezoelectric accelerometers of array 1 stopped working and for this reason some values are missing in the figure.
It can be noticed that along the array 1 only in two cases the peak acceleration ratio $a_{max}(z)/a_{max,i}$ was lower than 1, both at the ground surface, although along this array the peak acceleration at surface (A1) is generally lower than that measured along the array 2 (A7) . As in the case of horizontal barrier, it is confirmed also for the V-shaped barrier that the isolating effect generally decreases as the peak acceleration decreases. Contrarily to the results of the horizontal barrier, instead, the isolating effect increases as far as the nominal frequency of the input increases. A possible explanation is that the principal frequency of the isolated soil in the case of the V-shaped barrier is higher than in the model with the horizontal barrier, and likely closer to the frequency range of the input signals.
As mentioned above, the comparison with free-field conditions was again performed through numerical analyses.
Figure 16 shows the results in terms of ratio between the maximum acceleration on the surface of the model with ($a_{max,Vb}$) and without ($a_{max,ff}$) V-barrier, as a function of the peak input acceleration and of the principal frequency of the input signal. From this figure the effect of frequency, already commented above, is more evident: when the input frequency is small the values of the peak acceleration with and without soft barrier are very similar, while by increasing the input frequency the values become more and more distant.

CONCLUSIONS

This paper presents the results of an experimental work carried out in a geotechnical centrifuge. Two reduced scale models of soft barriers in a sand layer underwent a series of ground shaking. The aim of the study was to get experimental evidence of the capability of such soft barriers to isolate a volume of soil thus reducing ground amplification during ground motion caused by earthquakes.
The two models tested in centrifuge at 50g and 80g consisted each in a layer of dense Hostun sand, about 280 mm thick, free to be shaken along its main horizontal axis thanks to the adopted container (a laminar box). In the first model a thin horizontal layer made of latex balloons filled with a cross-linked gel was created at about mid-height of the sand layer. In the second, the same balloons were deployed to form a V-shaped barrier aimed at isolating a relatively shallow volume of sand. The former shape of treatment was chosen assuming that it can be more easily created in the site, compared to the deep horizontal layer. However, installation processes and relevant issues, such as the need to prevent or control excess static settlement during installation, were out of the scope of this piece of research.
The experimental results were compared with FE numerical analyses of the same models, carried out also in free field to have a benchmark condition. By validating the FE modelling via the comparison with the experimental results, a robust model has been built, that can be used for carrying out a wider parametric numerical testing.
The experimental results confirm the effectiveness of such soft barriers to reduce amplification in the isolated volume during seismic events. Despite the fact that the contrast of impedance between the sand and the barrier decreases because of the decay of sand shear stiffness with large strains, in stronger events the soft barrier shows its highest effectiveness. This is a clear evidence that yielding plays a beneficial role, and that a low shear strength is needed in the soft layer. Fortunately, Flora and Lombardi (submitted to Acta Geotechnica for possible publication) have shown that there is no need to have for it an extremely low value.
The effectiveness of V-shaped barriers is lower than that of the horizontal one. However, the latter should be considered just as a bounding reference conditions. Furthermore, the horizontal barrier isolates a continuous horizontal layer of sand having a mass larger than that bounded by the V-shaped barrier. Hence, the fundamental frequency of the V-shaped isolated volume is certainly higher that of the upper layer of soil in the test with horizontal barrier, closer to the frequency content of the input signals. This consideration is a possible explanation of the influence of the input signal frequency on the effectiveness of the V-shaped barrier emerged from the tests.
Even though the results shown in this and other papers are promising for the use of soft buried barriers, further efforts are needed before such a solution could be applied in the field. The main issues to tackle are the installation procedure and the subsequent settlements at ground level. Further engineering of the chemical composition of the soft material may be also required.

REFERENCES

Amorosi A., Boldini D., Elia G. (2010) Parametric studies on seismic ground responce by finite element modelling. Computers and Geotechnics, 515-528

Benz T. (2006). Small Strain Stiffness of Soil and its Numerical Consequences. Ph.d. thesis, Universitat Stuttgart

Benz T., Vermeer P.A., and Schwab R. (2009). A small-strain overlay model. Int J Num Anal Meth Geomech, 33(1), 25 - 44.

Brennan A.J., Madabhushi S.P.G., Houghton N.E., (2006). Comparing Laminar and ESB Containers for Dynamic Centrifuge Modelling. In: Physical Modelling in Geotechnics: ICPMG'06. Homg Kong: Balkema

Brennan A. J., Thusyanthan N. I., and Madabhushi S. P. G. (2005). Evaluation of shear modulus and damping in dynamic centrifuge tests. J. Geotech. Geoenviron. Eng., 131(12), 1488–1498.

Brinkgreve R. B, Kappert J M.H, Bonnier P.G.(2007) Hysteretic damping in a small-strain stiffness model. Numerical Models in Geomechanics NUMOG X Pande & Pietruszczak (eds) Taylor & Francis Group, London, ISBN 978-0-415-44027-1

Brinkgreve R.B.J., Swolfs W.M., and Engine E. (2011). PLAXIS user's manual, PLAXIS bv the Netherlands.

Chouw N., Schmid G. (1992). Building isolation using the transmitting behaviour of a soil layer. Proc. 10th World Conference on Earthquake Engineering, Madrid (Spain), 4: 2519-2524

Flavigny E., Desrues J., Palayer B. (1990). Note Technique le sable d' Hostun "RF". Rev. Franc. Geotech. N°53 pp. 67-70

Flora A., Bilotta E., Lirer L., Lombardi D., Nappa V. (2015). Behavior of a sand-polyacrilate mixture. Proc. Sixth International Symposium on Deformation Characteristics of Geomaterials, Buenos Aires (Argentina).

Ghosh B., and Madabhushi S. P. G. (2002). An efficient tool for measuring shear wave velocity in the centrifuge. Proc. Int. Conf. on Phys. Modelling in Geotechnics, R. Phillips, P. J. Guo, and R. Popescu, eds.,Balkema, Rotterdam, Netherlands, 119–124.

Hardin B.O., Black W.L. (1969) Closure to vibration modulus of normally consolidated clays Proc. ASCE: Journal of the Soil Mechanics and Foundation Divisio, 95 (SM6): 1531-1537

Hing-Ho Tsang, S. H. Lo, X. Xu1, M. Neaz Sheikh (2012). Seismic isolation for low-to-medium-rise buildings using granulated rubber–soil mixtures: numerical study. Earthquake Engineering & Structural Dynamics; 41:2009–2024

Hoque E., Tatsuoka F.(2004). Effects of stress ratio on small-strain stiffness during triaxial shearing. Geotechnique, 54 (7):429-439.

Kellezi L. (2011). Dynamic behavior of a softer layer overlying hard soil / bedrock and vibration reduction. GEO-Danish Geotechnical Institute, Lyngby (Danmark).

Kirtas E, Rovithis E, Pitilakis K (2009a). Subsoil interventions effect on structural seismic response. Part I: validation of numerical simulations. Journal of Earthquake Engineering; 13(2):155–169.

Kirtas E, Pitilakis K. (2009b) Subsoil interventions effect on structural seismic response. Part II: parametric investigation. Journal of Earthquake Engineering; 13(3):328–344.

Lanzano G., Bilotta E., Russo G., Silvestri F., Madabhushi S.P.G. (2012). Centrifuge modeling of seismic loading on tunnels in sand. Geotechnical Testing Journal, 35(6) 854-869. DOI: 10.1520/GTJ104348

Lanzano G., Bilotta E., Russo G., Silvestri F. (2015). Experimental and numerical study on circular tunnels under seismic loading. European Journal of Environmental and Civil Engineering, 19 (5) 539-563. DOI: 10.1080/19648189.2014.893211

Liao S, Sangrey DA (1978). Use of piles as isolation barriers. Journal of the Geotechnical Engineering Division (ASCE); 104(GT9):1139–1152.

Lombardi D. (2014). An innovative ground treatment approach for seismic risk mitigation of existing structures. Ph.D. Thesis, University of Napoli Federico II (Italy).

Lombardi D., Flora A., Lirer S., Silvestri F. (2014). Soil grouting for the seismic protection of existing buildings. Proceedings of the Institution of Civil Engineers: Ground Improvement, 167 (3), pp. 206-218. DOI: 10.1680/grim.13.00010

Madabhushi S.P.G., Schofield A.N., Lesley S., (1998) A New Stored Angular Momentum (SAM) Based Earthquake Actuator. In: Proc. Centrifuge '98. Tokyo, Japan: Balkema

Madabhushi S.P.G., Houghton, N.E. & Haigh, S.K. (2006). A new automatic sand pourer for model preparationat University of Cambridge. Int. Conf. on Physical Modelling in Geotechnics, Hong Kong, 3–8 August: 217–222. Rotterdam: Balkema.

Madabhushi S.P.G. (2014). Centrifuge modelling for Civil Engineers, Spon Press, ISBN-10: 567 0415668247

Massarsch K. R. (2003). Mitigation of Traffic-induced Ground Vibrations. 11th Int.Conference on Soil Dynamics and Earthquake Engineering (ICSDEE) and The Third International Conference on Earthquake Geotechnical Engineering (ICEGE), 7 – 9th January,2004, Berkeley, California, 1: 22 31.

Massarsch K. R. (2005). Ground Vibration Isolation Using Gas-filled Cushions. Proc. of the International Workshop on the Mitigation and Countermeasures of Ground Environment, IW525SHIGA 2005, 123 – 133.

Park D., Hashash Y. M. A. (2004). Soil damping formulation in nonlinear time domain site response analysis. Journal of Earthquake Engineering, 8, 49–274.

Santos JA, Correia, AG (2001) Reference threshold shear strain of soil. Its application to obtain an unique strain-dependent shear modulus curve for soil. In 15th Int. Conf. SMGE, volume 1,pp 267-270, Istanbul: Balkema

Schanz T., Vermeer P.A., and Bonnier P.G. (1999). The hardening soil model: formulation and verification. In Beyond 2000 in computation geotechnics (ed. R. B. J. Brinkgreve), pp. 281–290. Rotterdam: Balkema.

Scott R.F, (1994) Review of Progress in Dynamic Geotechnical Centrifuge Research. In: R.J. Ebleher, V.P. Drnevich, and B.L.Kutter, eds. Dynamic Geotechnical Testing II, ASTM STP 1213. San Francisco : ASTM.

Woods RD. (1968) Screening of surface waves in soils. Journal of the Soil Mechanics and Foundations Division (ASCE); 94(SM4):951–979.

Yegian MK, Kadakal U. (2004) Foundation isolation for seismic protection using a smooth synthetic liner. Journal of Geotechnical and Geoenvironmental Engineering (ASCE);130(11):1121–1130.

Zeghal M., Elgamal A. W., Zeng X., and Arulmoli K. (1999). Mechanism of liquefaction response in sand-silt dynamic centrifuge tests. Soil Dyn. Earthquake Eng., 18(1), 71–85

Fig. 1a

Click here to download line figure Figure 1a.tiff

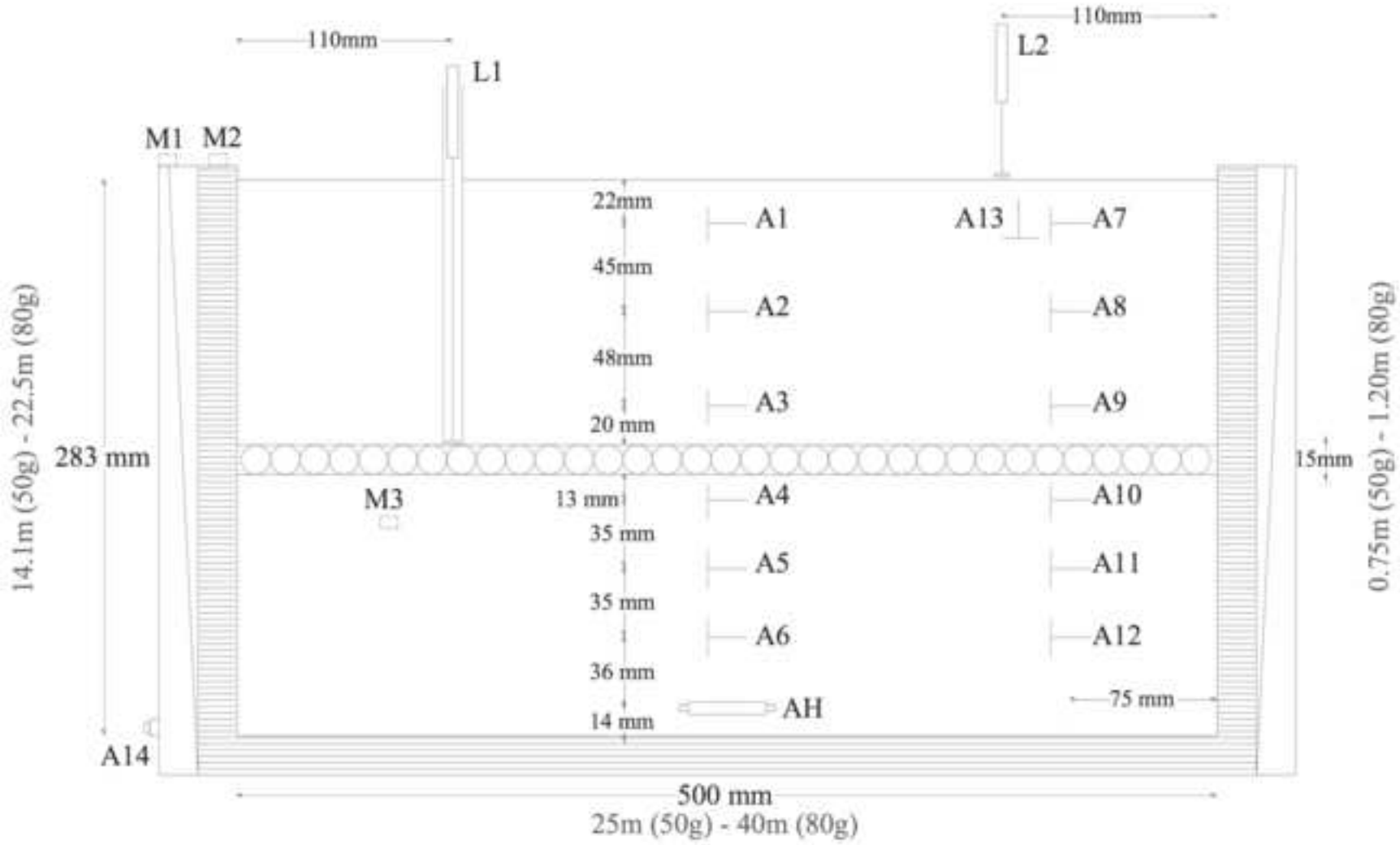

A : Piezoelectric Accelerometers
M: Microelectromechanical System Accelerometer
L: Linear Variable Differential Transformer
AH: Air Hammer Piezoelectric Accelerometer

Fig. 1b

Click here to download line figure Figure 1b.tiff

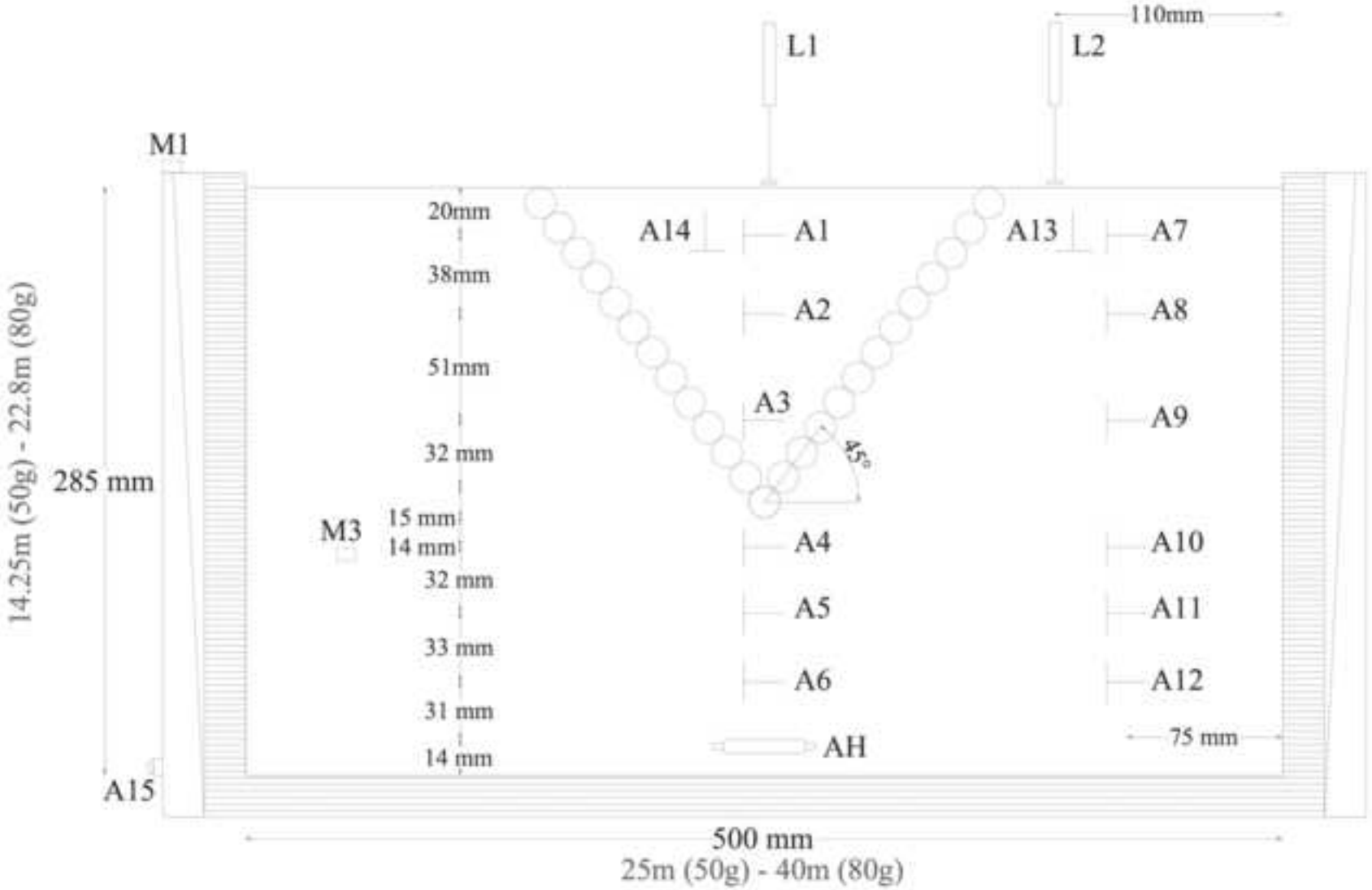

Fig. 2

Click here to download line figure Figure 2.tiff

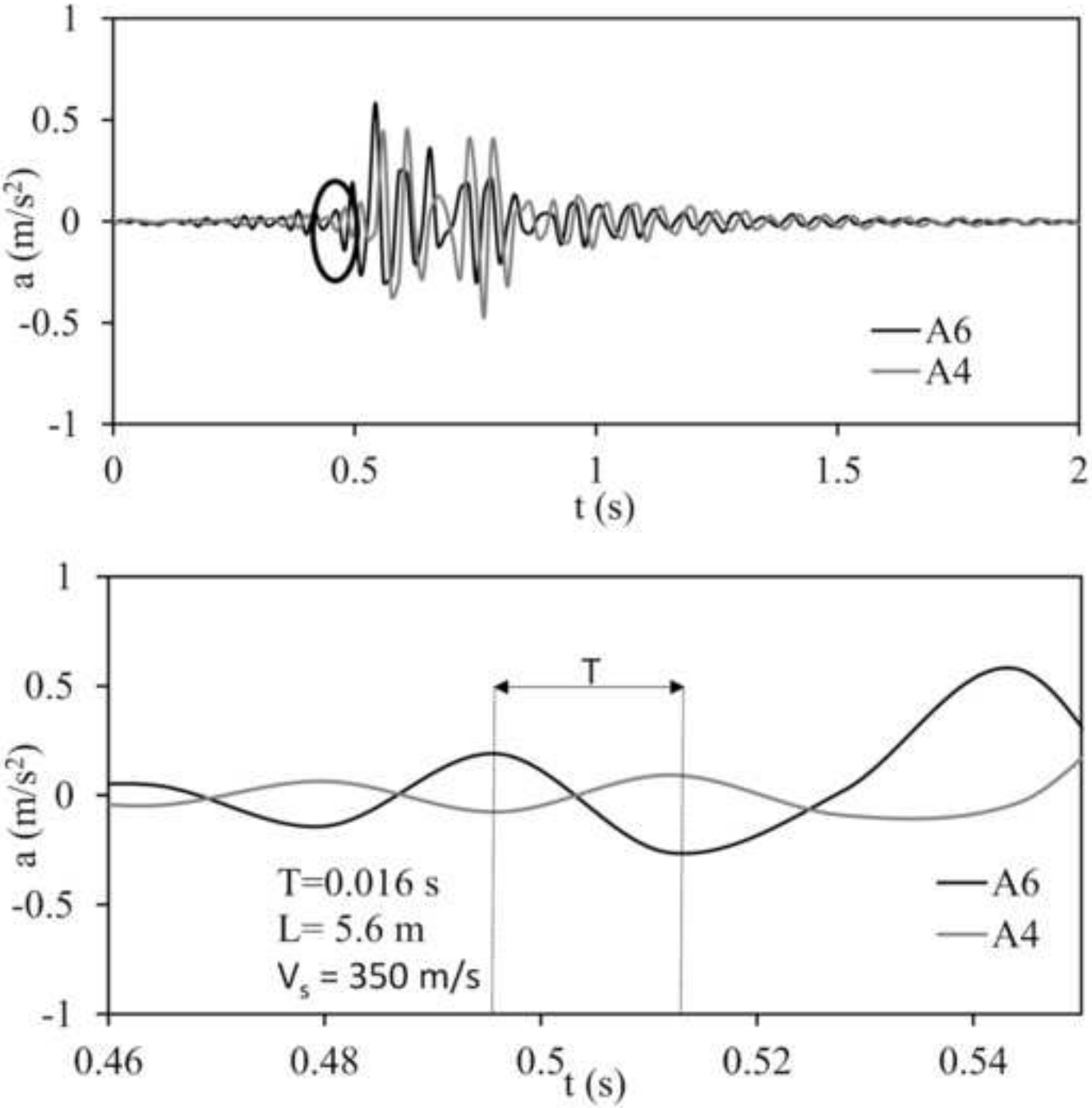

Fig. 3

Click here to download line figure Figure 3.tiff

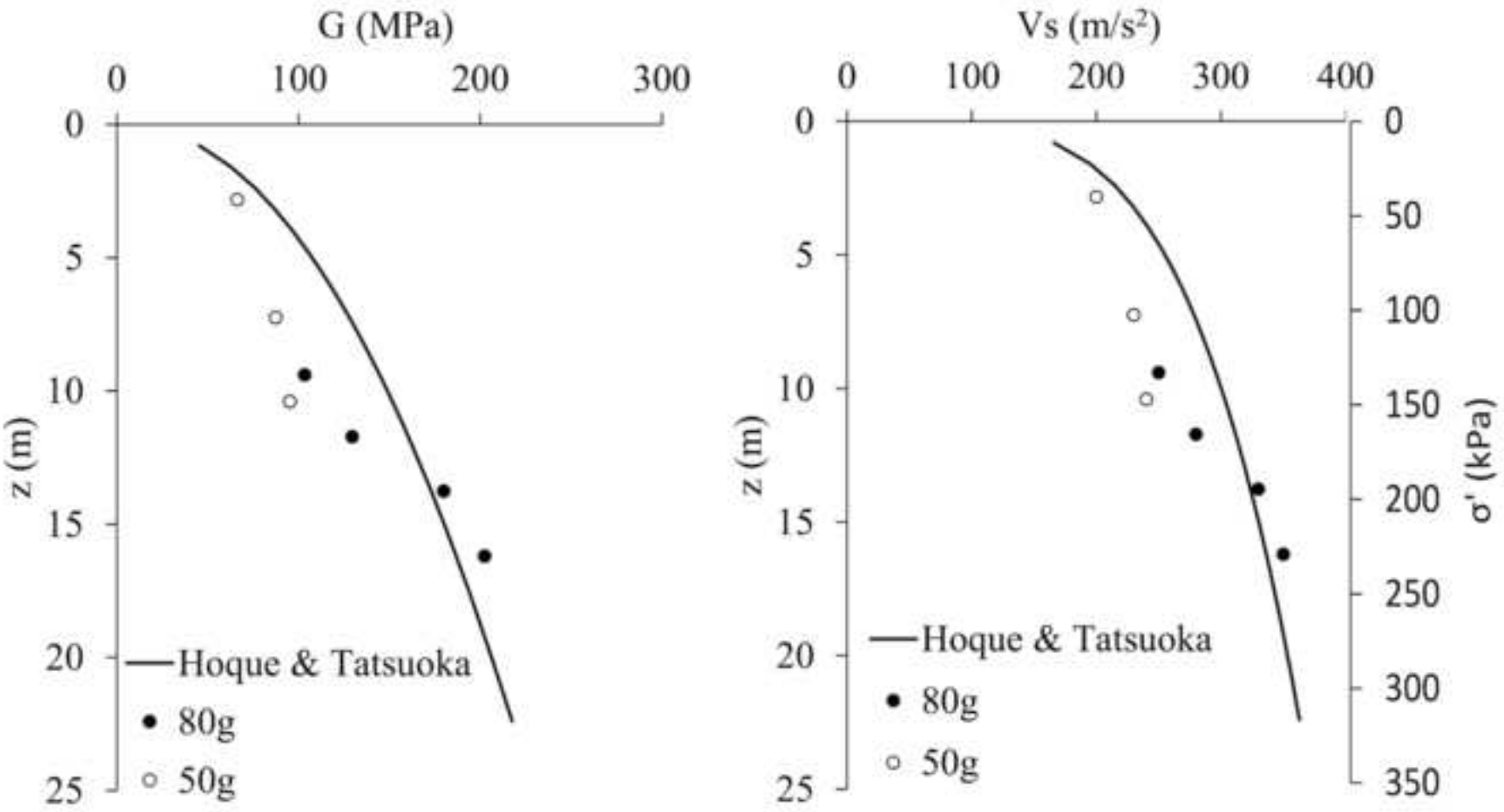

Fig. 4

Click here to download line figure Figure 4.tiff

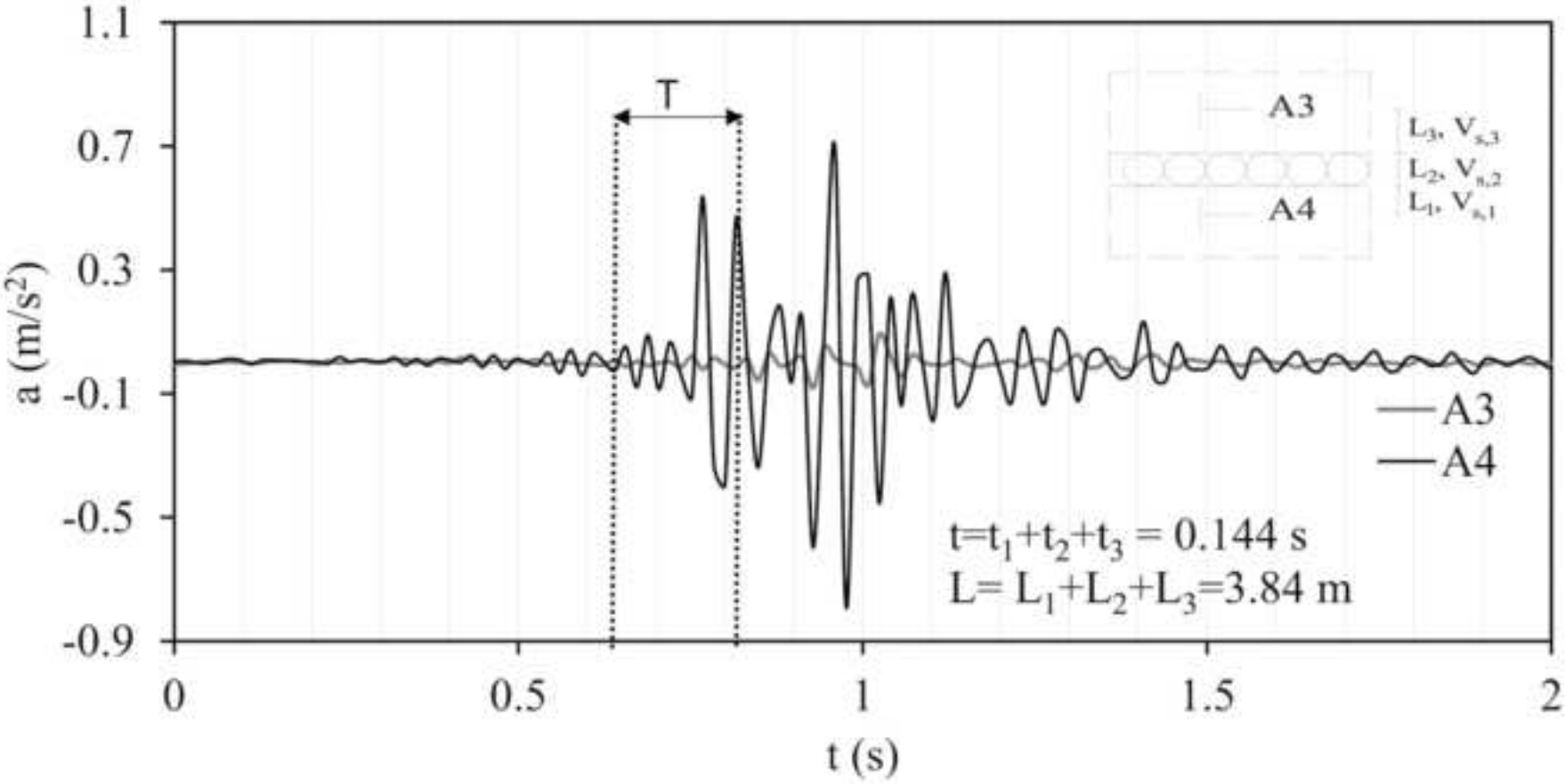

Fig. 5

Click here to download line figure Figure 5.tiff

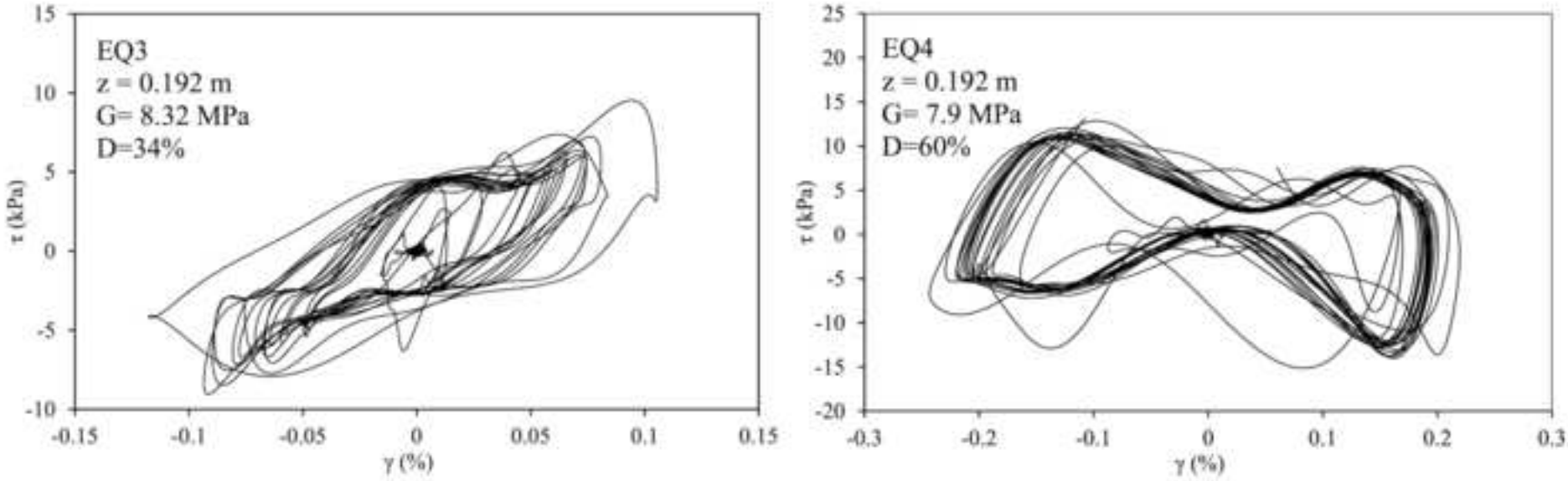

Fig. 6

Click here to download line figure Figure 6.tiff

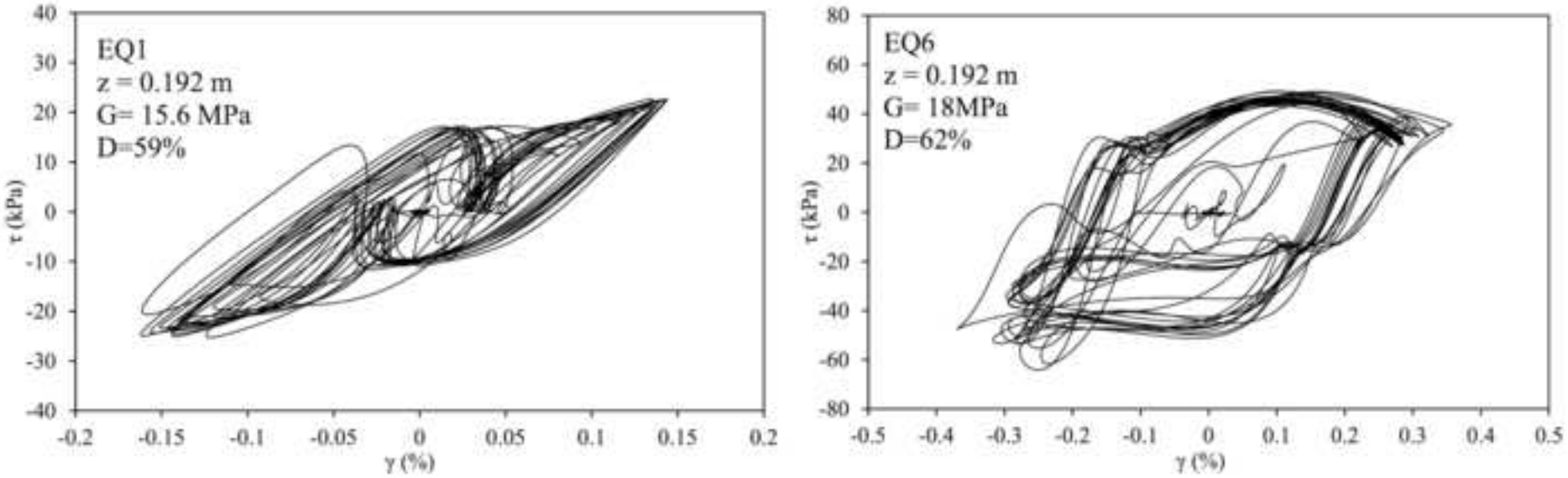

Fig. 7

Click here to download line figure Figure 7.tiff

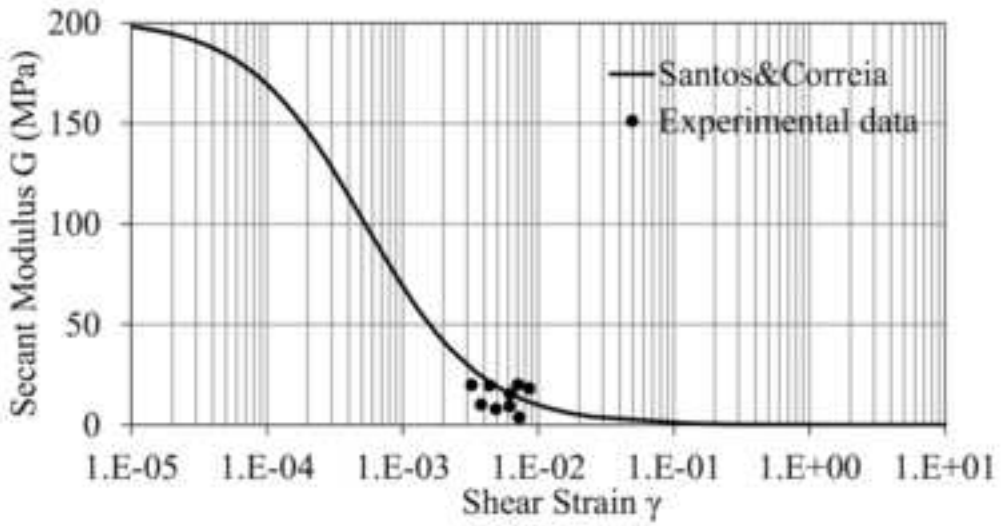

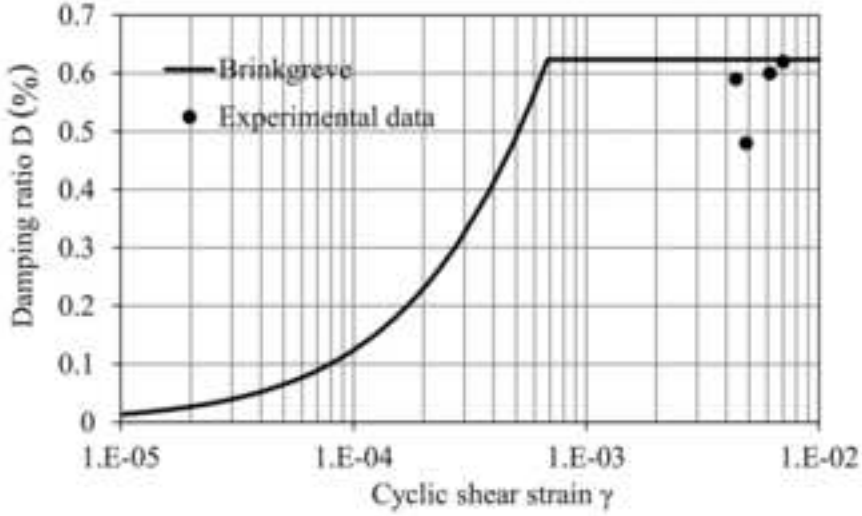

Fig. 8a

Click here to download line figure Figure 8a.tiff

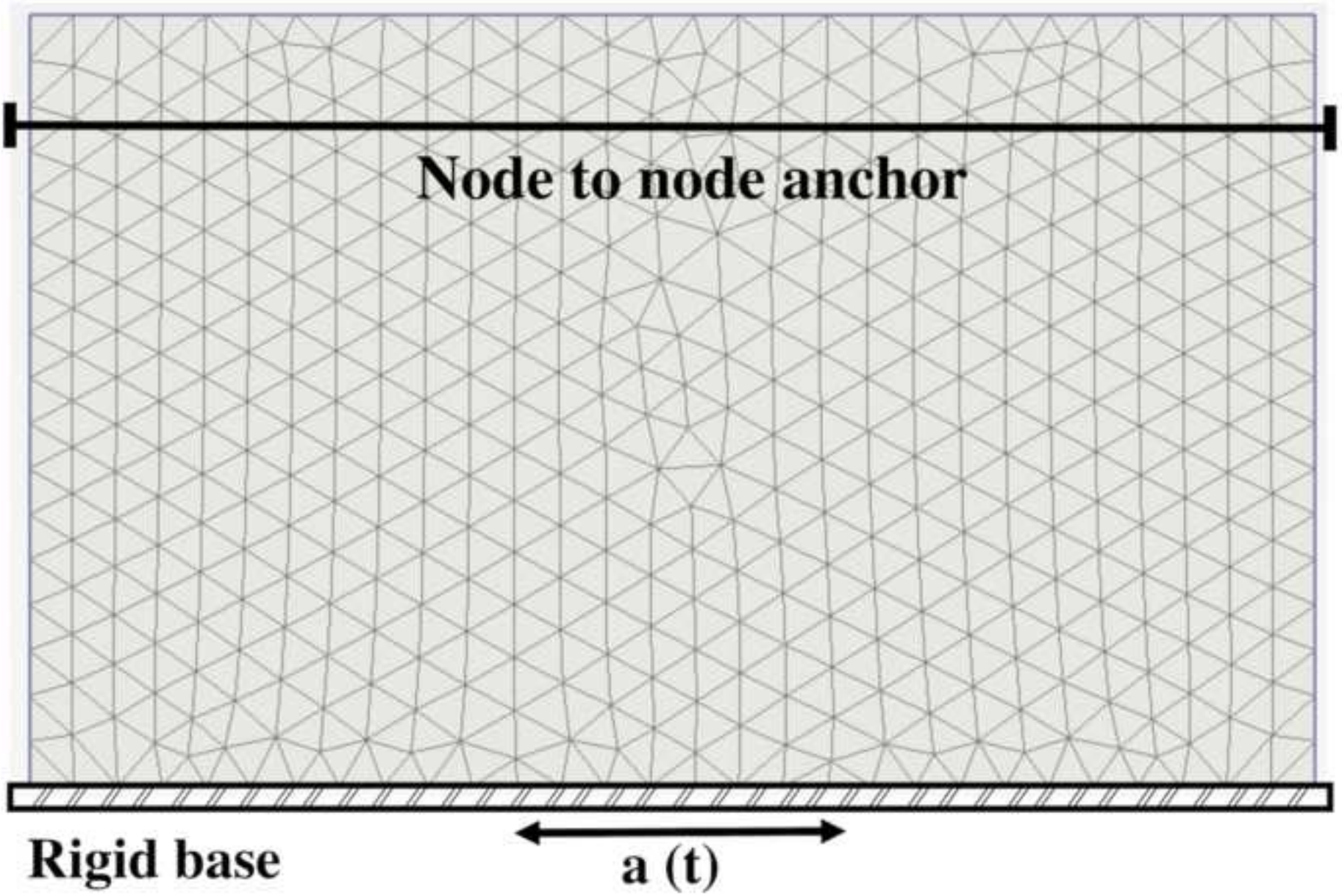

Fig. 8b

Click here to download line figure Figure 8b.tiff

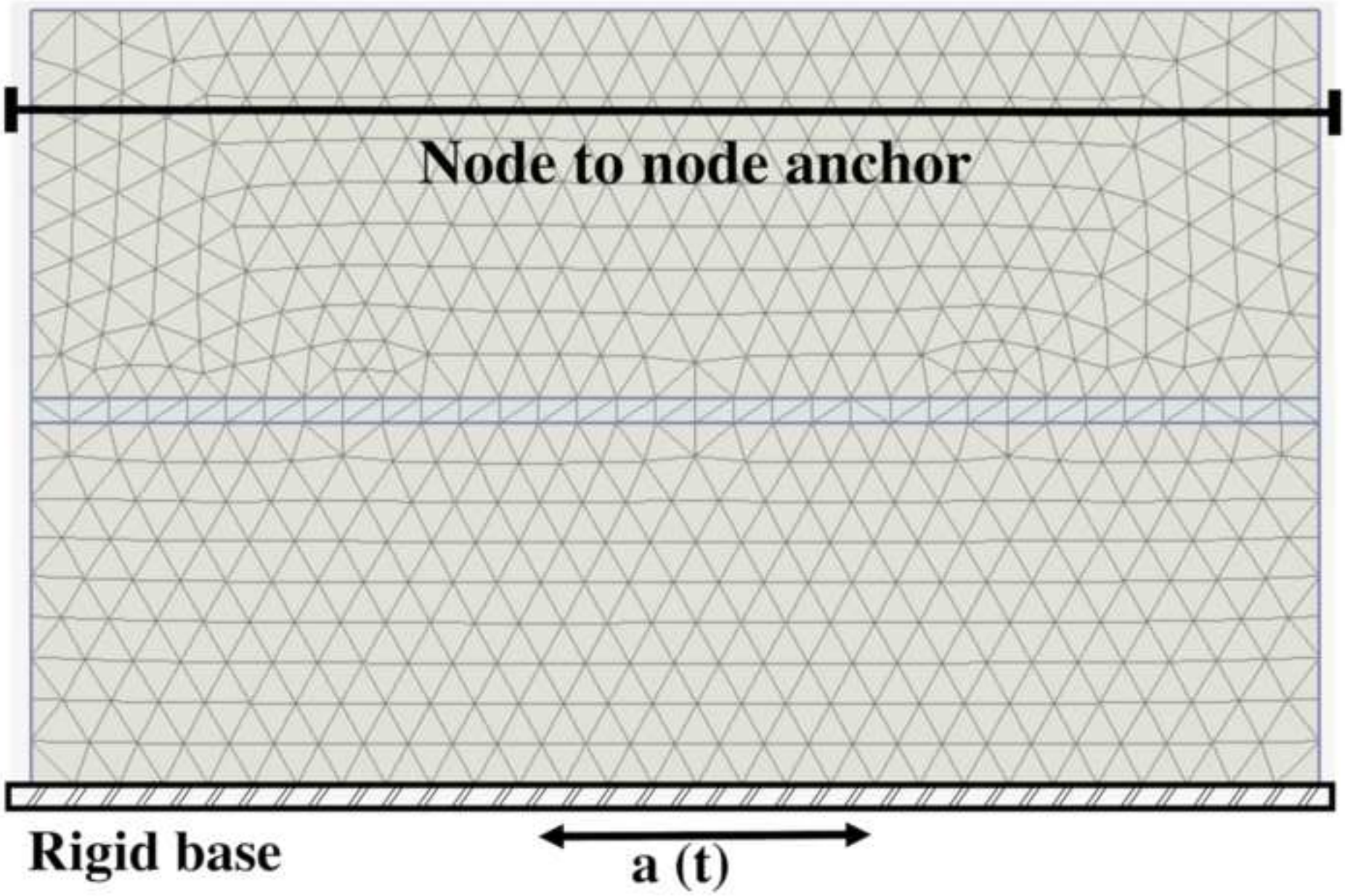

Fig. 8c

Click here to download line figure Figure 8c.tiff

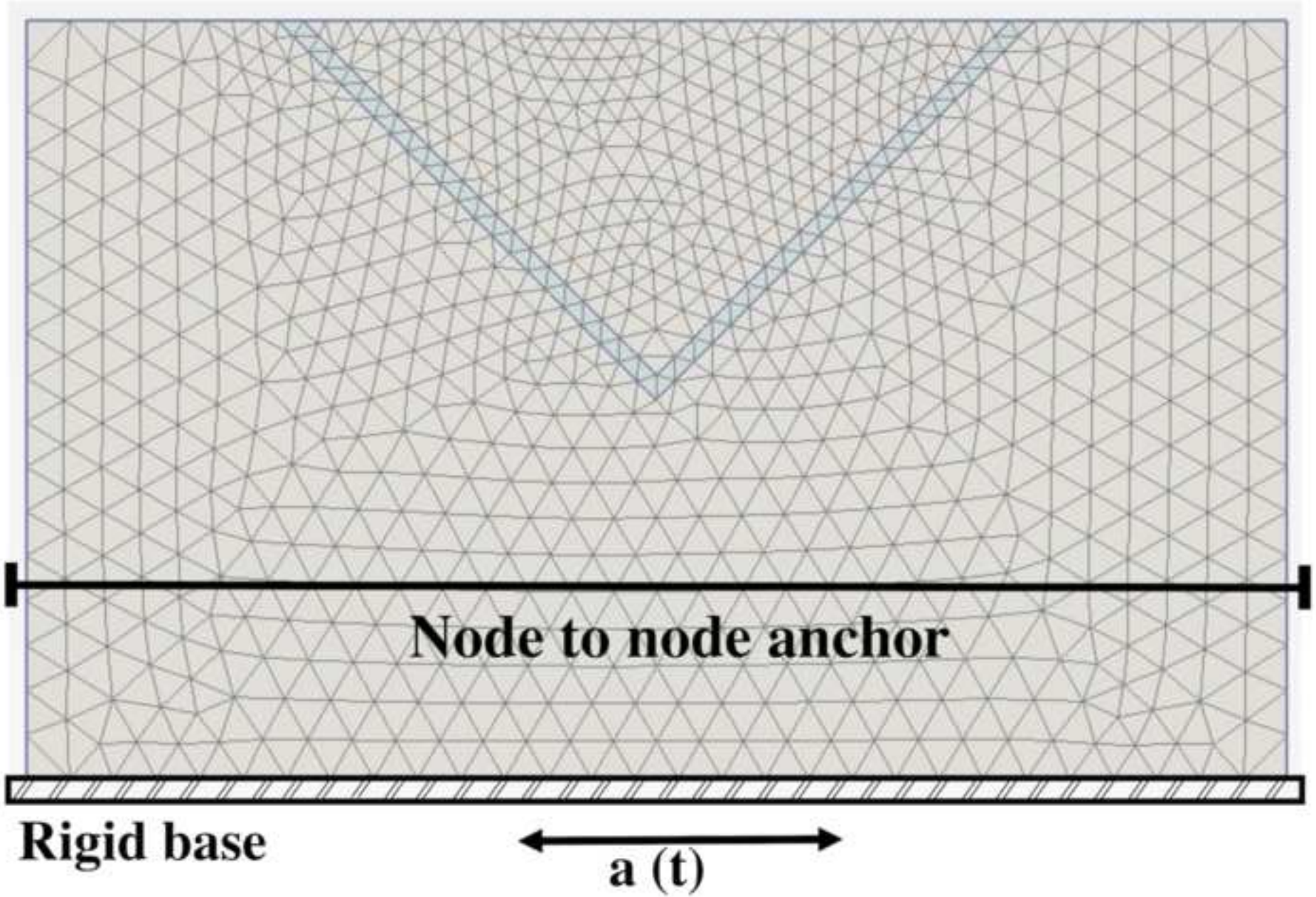

Fig. 9

Click here to download line figure Figure 9.tiff

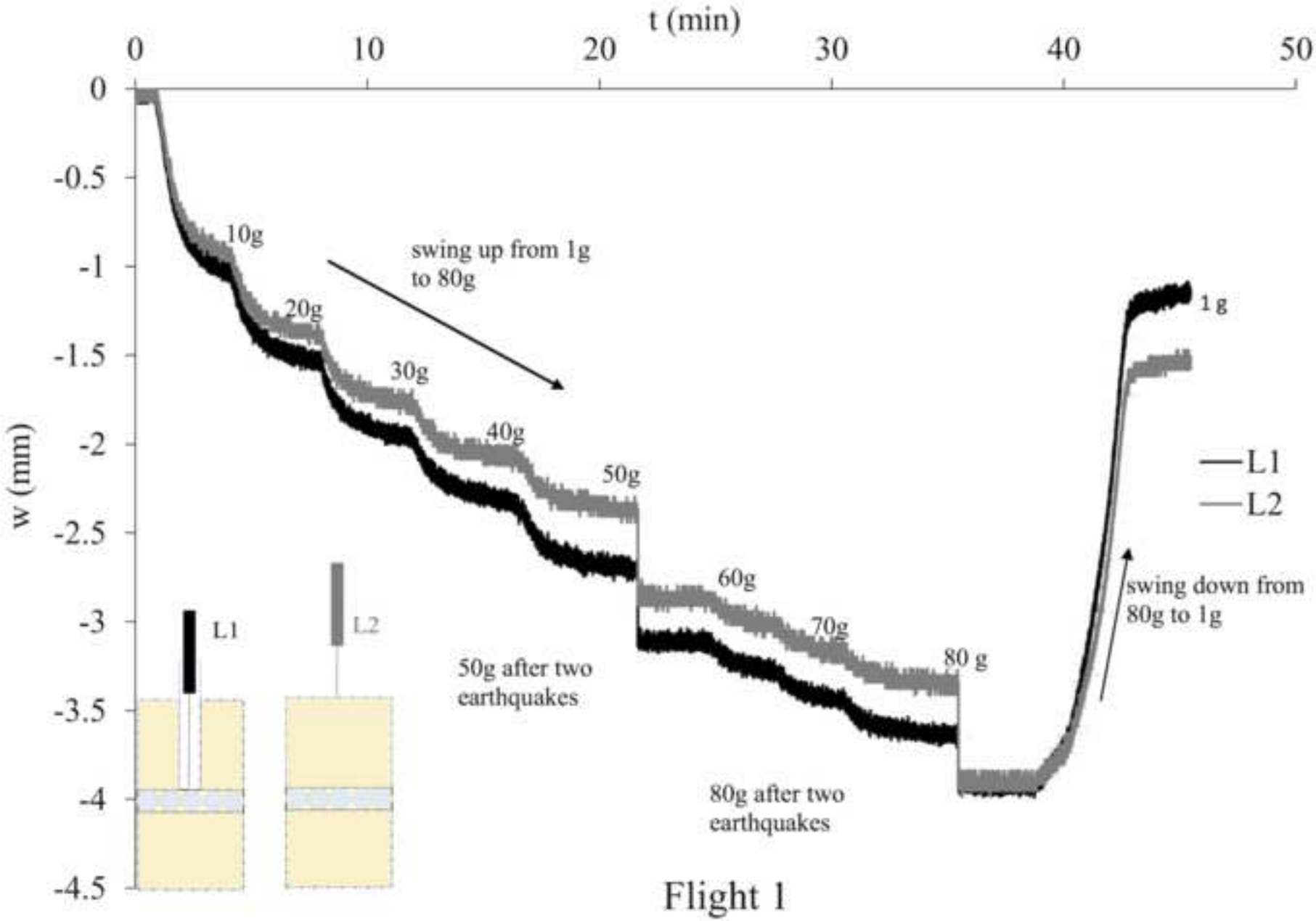

Fig. 10

Click here to download line figure Figure 10.tiff

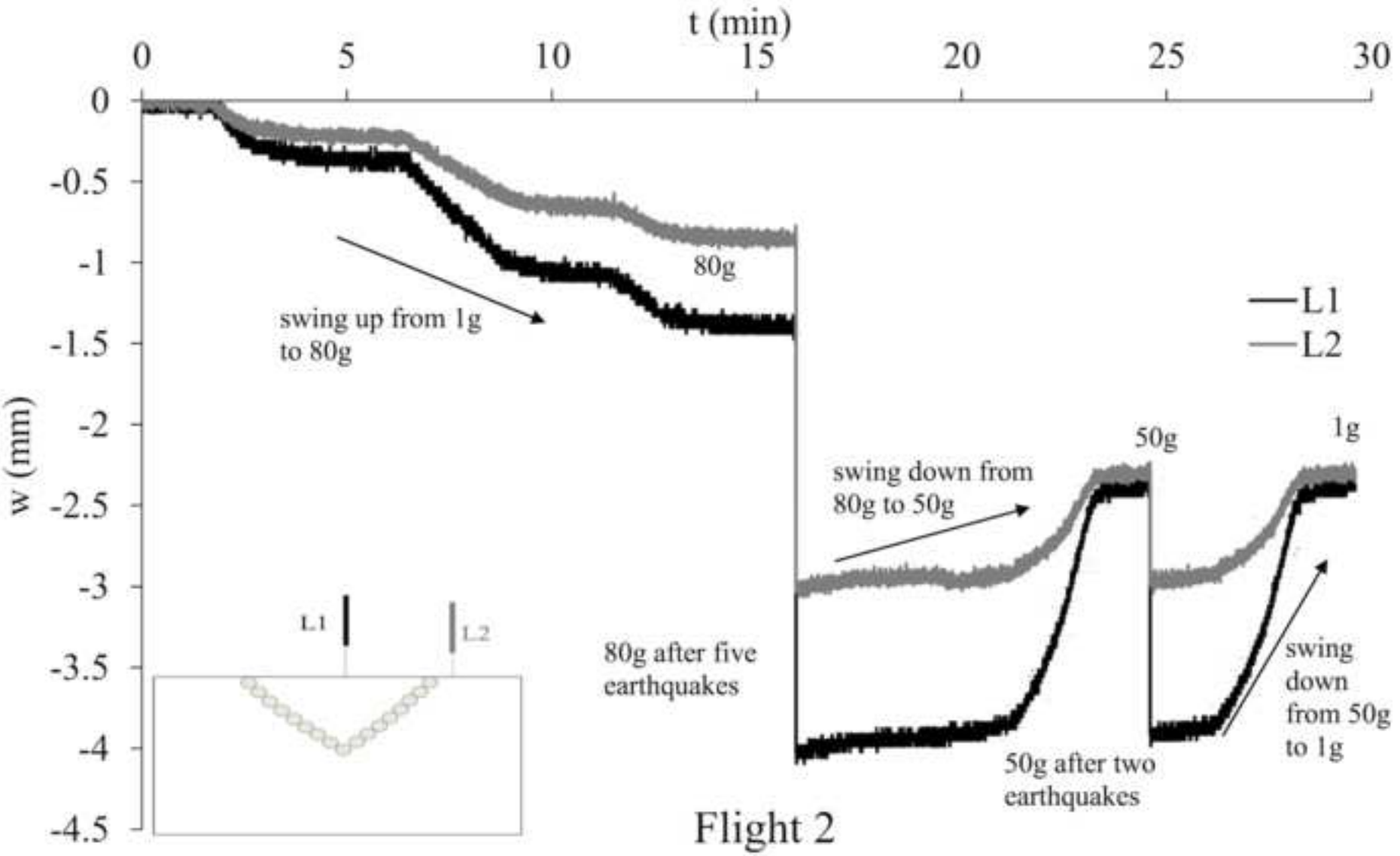

Fig. 11

Click here to download line figure Figure 11.tiff

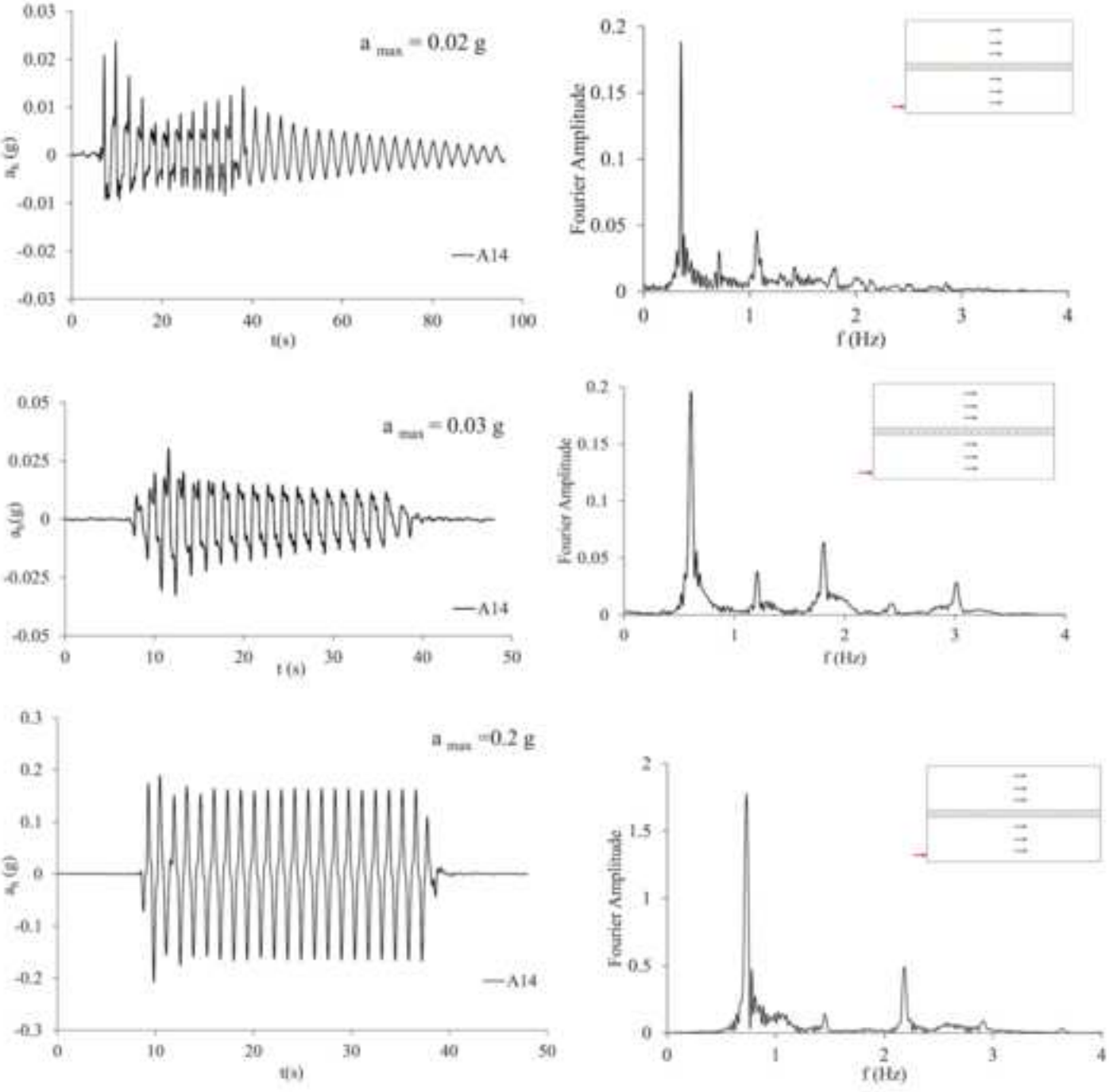

Fig. 12

Click here to download line figure Figure 12.tiff

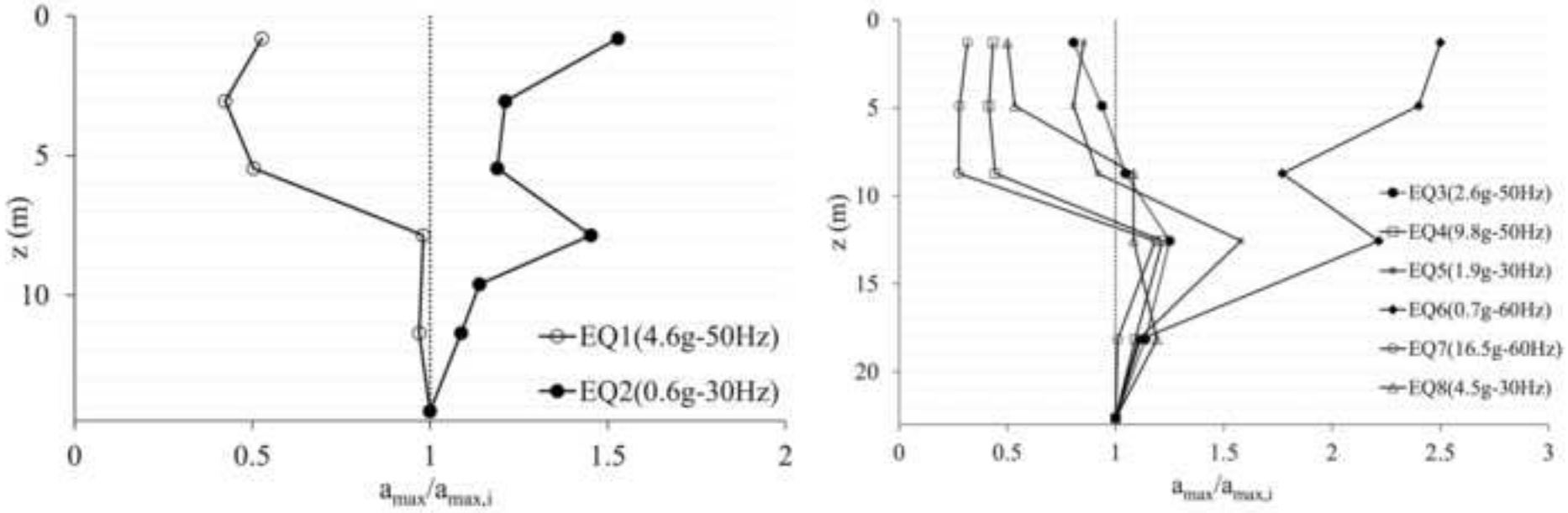

Fig. 13

Click here to download line figure Figure 13.tiff

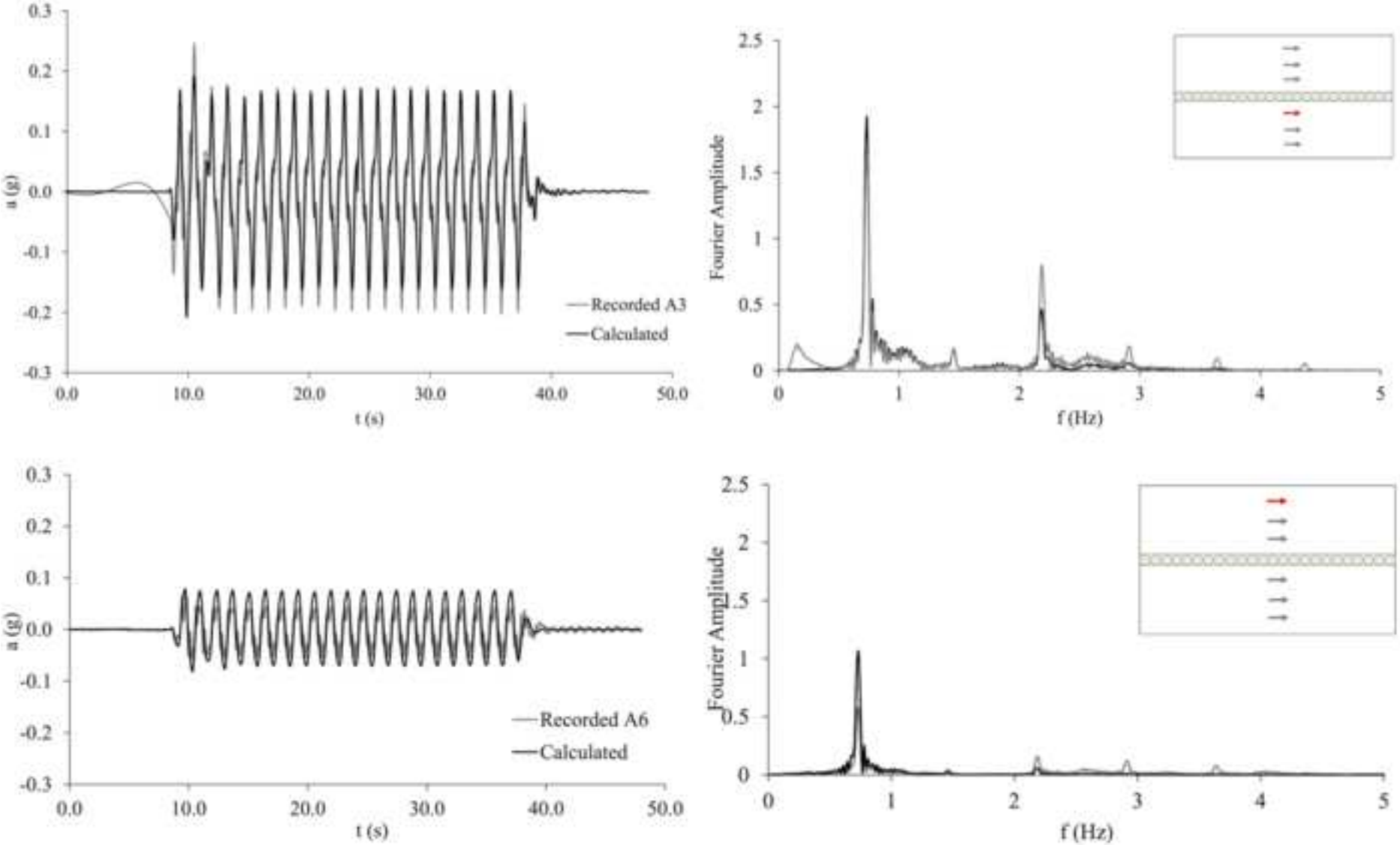

Fig. 14a

Click here to download line figure Figure 14a.tiff

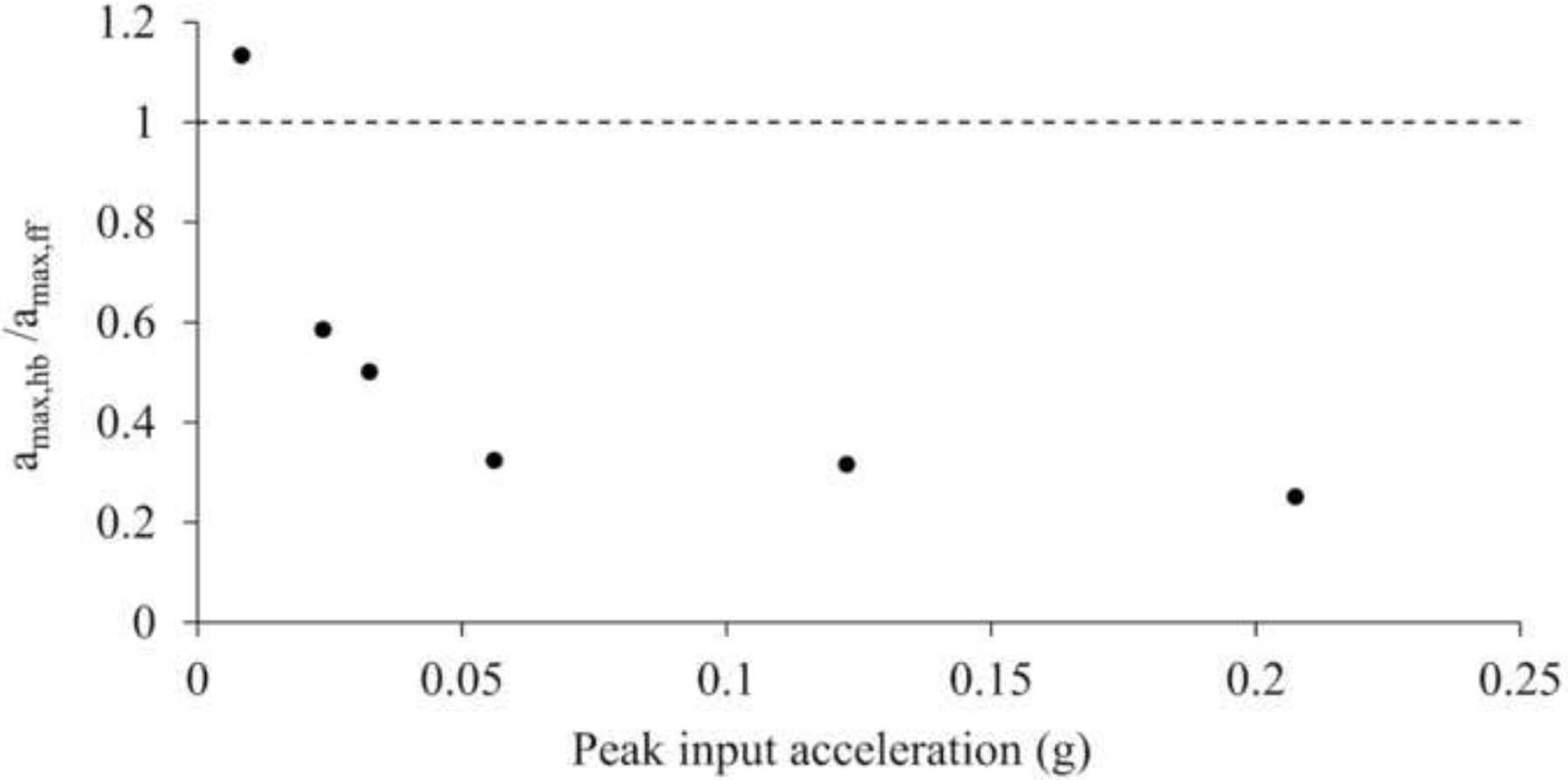

Fig. 14b

Click here to download line figure Figure 14b.tiff

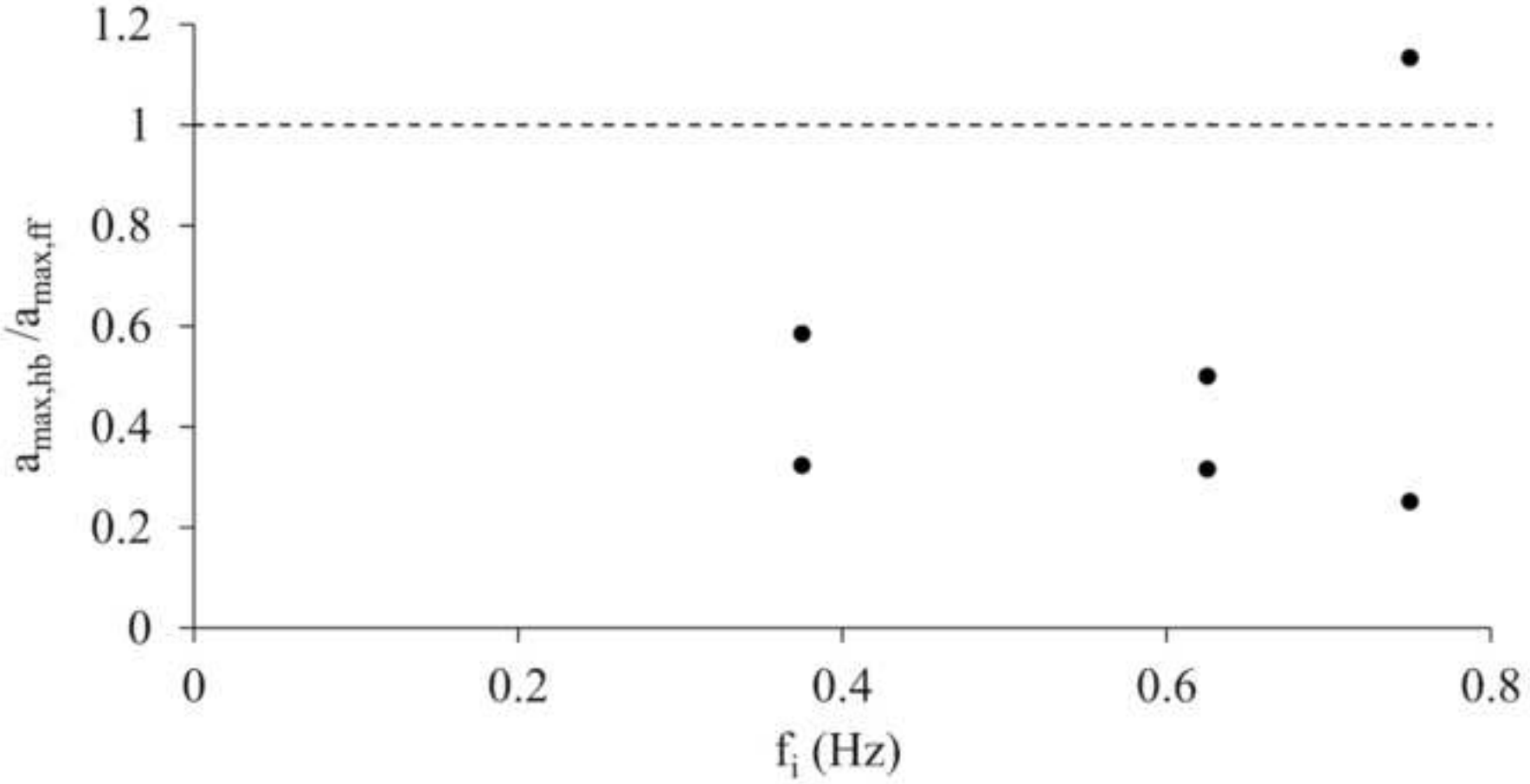

Fig. 15

Click here to download line figure Figure 15.tiff

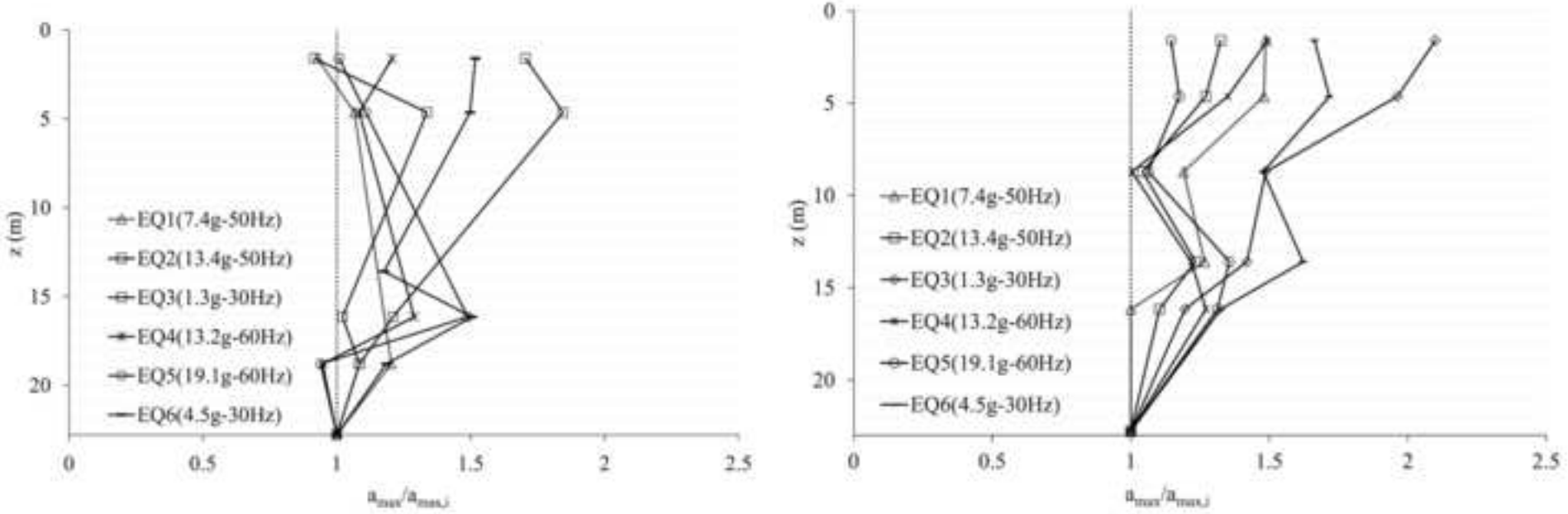

Fig. 16

Click here to download line figure Figure 16.tiff